Appl. Phys. A (2016) 122:158
DOI 10.1007/s00339-016-9643-4

Applied Physics A
Materials Science & Processing

Efficient computation of the spontaneous decay rate of arbitrarily shaped 3D nanosized resonators: a Krylov model-order reduction approach

Jörn Zimmerling[1] · Lei Wei[2] · Paul Urbach[2] · Rob Remis[1]

Received: 14 August 2015 / Accepted: 18 November 2015 / Published online: 18 February 2016

Abstract We present a Krylov model-order reduction approach to efficiently compute the spontaneous decay (SD) rate of arbitrarily shaped 3D nanosized resonators. We exploit the symmetry of Maxwell's equations to efficiently construct so-called reduced-order models that approximate the SD rate of a quantum emitter embedded in a resonating nanostructure. The models allow for frequency sweeps, meaning that a *single* model provides SD rate approximations over an entire spectral *interval* of interest. Field approximations and dominant quasinormal modes can be determined at low cost as well.

1 Introduction

The spontaneous decay (SD) rate of a quantum emitter depends on its environment and can be modified by an electromagnetic resonance. This so-called Purcell effect [1] is a basic effect in quantum electrodynamics, and it is well known that in the so-called weak-coupling regime, the SD rate can be computed classically and does not require a quantum mechanical treatment. Specifically, for electric-dipole transitions that take place at $\mathbf{r} = \mathbf{r}_0$, the SD rate γ normalized with respect to the decay rate γ_0 in a reference medium can be computed as [2]

$$\gamma/\gamma_0 = P/P_0, \tag{1}$$

where

$$P = \frac{\omega}{2} yIm[\mathbf{p}^* \cdot \mathbf{E}(\mathbf{r}_0)] \tag{2}$$

is the power radiated by an electric dipole of the form $\hat{\mathbf{J}}^{\text{ext}} = -\mathrm{i}\omega\mathbf{p}\delta(\mathbf{r} - \mathbf{r}_0)$ with $\mathbf{p}$ the dipole moment and P_0 is the radiated power in the reference medium.

To determine the SD rate, the electric field at the location of the quantum emitter is required over a spectral interval of interest. For emitters located in the vicinity of dispersive nanostructures, we therefore have to solve the Maxwell equations

$$-\nabla \times \hat{\mathbf{H}} - \mathrm{i}\omega\hat{\mathbf{D}} = -\hat{\mathbf{J}}^{\text{ext}} \tag{3}$$

and

$$\nabla \times \hat{\mathbf{E}} - \mathrm{i}\omega\mu_0\hat{\mathbf{H}} = \mathbf{0}, \tag{4}$$

where $\hat{\mathbf{D}} = \varepsilon\hat{\mathbf{E}} + \tilde{\mathbf{P}}$ with $\varepsilon = \varepsilon_0\varepsilon_\infty$ and ε_∞ is the instantaneous (high-frequency) relative permittivity. For dispersive Drude or Lorentz materials, $\tilde{\mathbf{P}}$ satisfies the constitutive relation

$$-\omega^2\tilde{\mathbf{P}} - \mathrm{i}\omega\beta_2\tilde{\mathbf{P}} + \beta_1\tilde{\mathbf{P}} = \beta_0\hat{\mathbf{E}}, \tag{5}$$

where the coefficients β_i are determined by the type of dispersive material that is considered. In particular, for a Drude material, we have $\beta_0 = \varepsilon_0\omega_\mathrm{p}^2$, $\beta_1 = 0$, and $\beta_2 = \gamma_\mathrm{p}$, where ω_p is the volume plasma frequency and γ_p the collision frequency, while for a Lorentz material we have $\beta_0 = \varepsilon_0(\varepsilon_\mathrm{s} - \varepsilon_\infty)\omega_0^2$, $\beta_1 = \omega_0^2$, and $\beta_2 = 2\delta$, where ε_s is the static relative permittivity, ω_0 the resonant plasma frequency, and δ the damping constant.

Introducing now the auxiliary field variable $\hat{\mathbf{U}} = \mathrm{i}\omega\tilde{\mathbf{P}}$, Maxwell's Eq. (3) and (4) and the constitutive relation (5) can be combined and written in first-order form as

✉ Jörn Zimmerling
J.T.Zimmerling@TUDelft.NL

[1] Circuits and Systems Group, Delft University of Technology, Delft, The Netherlands

[2] Optics Research Group, Delft University of Technology, Delft, The Netherlands

$$(\mathcal{D} + \mathcal{S} - \mathrm{i}\omega\mathcal{M})\mathcal{F} = \mathcal{Q}', \tag{6}$$

where $\mathcal{D}$ contains the curl operators, $\mathcal{S}$ and $\mathcal{M}$ are medium matrices, and $\mathcal{F}$ and $\mathcal{Q}'$ are the field and source vectors, respectively. To determine the projection of the electric field strength onto the dipole moment $\mathbf{p}$ at the location of the quantum emitter, we need to solve the above first-order Maxwell system and extract the electric field strength components at the emitter location from the field vector $\mathcal{F}$. This can be realized in a very efficient manner for arbitrary three-dimensional geometries using a Krylov subspace model-order reduction method.

2 Krylov model-order reduction

To efficiently construct Krylov subspace SD rate approximants, we first discretize Eq. (6) in space on a standard second-order finite-difference grid (Yee grid [3]) and apply the optimal complex-scaling method proposed in [4] and extended in [5] to simulate the extension to infinity. After these two steps, we arrive at the large-scale semidiscrete Maxwell system

$$(\mathsf{D} + \mathsf{S} - \mathrm{i}\omega\mathsf{M})\mathsf{f}_{\mathrm{cs}} = \mathsf{q}', \tag{7}$$

where D, S, M, f_{cs}, and q' are the discretized counterparts of $\mathcal{D}$, $\mathcal{S}$, $\mathcal{M}$, $\mathcal{F}$, and $\mathcal{Q}'$, respectively, and the subscript "cs" indicates that complex-scaling has been applied. The order n of the discretized system is typically very large and can easily run into the millions especially for three-dimensional problems.

The Maxwell system of Eq. (7) cannot be used directly to determine the electromagnetic field, since causality is lost due to the application of the complex-scaling method (see [4–6]). However, if we introduce the so-called system matrix as $\mathsf{A} = \mathsf{M}^{-1}(\mathsf{D} + \mathsf{S})$, then stable time-domain or conjugate-symmetric frequency-domain field approximations can be constructed via a stability-correction procedure as described in [4]. In particular, for an electric-dipole moment vector of the form $\mathbf{p} = p(\omega)\mathbf{n}$, where $\mathbf{n}$ is a unit vector, the frequency-domain field can be computed via

$$\mathsf{f}(\omega) = \mathrm{i}\omega p(\omega)[r(\mathsf{A}, \omega) + r(\mathsf{A}^*, \omega)]\mathsf{M}^{-1}\mathsf{q}, \tag{8}$$

where q is a finite-difference approximation of $\mathbf{n}\delta(\mathbf{r} - \mathbf{r}_0)$ and

$$r(z, \omega) = \frac{\eta(z)}{z - \mathrm{i}\omega} \tag{9}$$

with $\eta(z)$ the complex Heaviside unit step function given by

$$\eta(z) = \begin{cases} 1 & \text{for } \mathrm{Re}(z) > 0, \\ 0 & \text{for } \mathrm{Re}(z) < 0. \end{cases} \tag{10}$$

Direct evaluation of Eq. (8) is not feasible, however, since the order of the system matrix A is simply too large. Fortunately, it can be shown that the system matrix satisfies the symmetry relation

$$\langle \mathsf{Ax}, \mathsf{y} \rangle = \langle \mathsf{x}, \mathsf{Ay} \rangle \quad \text{for all } \mathsf{x}, \mathsf{y} \in \mathbb{C}^n, \tag{11}$$

where $\langle \cdot, \cdot \rangle$ is a bilinear form given by $\langle \mathsf{x}, \mathsf{y} \rangle = \mathsf{y}^T\mathsf{WMx}$ with WM complex-symmetric and W a step size matrix containing the step sizes of the computational grid (see [7]). This property allows us to carry out a Lanczos-type reduction algorithm [7, 8] to efficiently compute frequency-domain field approximations and the corresponding SD rate. Specifically, with the source vector $\mathsf{M}^{-1}\mathsf{q}$ as a starting vector, we obtain after $m \ll n$ steps of the Lanczos algorithm the sequence of vectors v_1, v_2, ...,v_m that form a basis of the Krylov subspace

$$\mathbb{K}_m = \mathrm{span}\{\mathsf{M}^{-1}\mathsf{q}, \mathsf{AM}^{-1}\mathsf{q}, \ldots, \mathsf{A}^{m-1}\mathsf{M}^{-1}\mathsf{q}\}. \tag{12}$$

These m steps can be summarized as

$$\mathsf{AV}_m = \mathsf{V}_m\mathsf{H}_m + \mathsf{p}_{m+1}\mathsf{e}_m^T, \tag{13}$$

where V_m is a tall n-by-m matrix having the basis vectors v_i as its columns, H_m is an m-by-m tridiagonal matrix containing the Lanczos recurrence coefficients, p_{m+1} is a residual vector, and e_m is the mth column of the m-by-m identity matrix I_m. We note that large-scale SD rate problems can be handled by our reduction method, since only three basis vectors need to fit inside the memory of the computational architecture due to the 3-term Lanczos recurrence relation.

With the so-called Lanczos decomposition of Eq. (13) at our disposal, the reduced-order model for the frequency-domain electromagnetic field now follows as

$$\mathsf{f}_m(\omega) = \mathrm{i}\omega p(\omega)\|\mathsf{M}^{-1}\mathsf{q}\|\left[\mathsf{V}_m r(\mathsf{H}_m, \omega) + \mathsf{V}_m^* r(\mathsf{H}_m^*, \omega)\right]\mathsf{e}_1, \tag{14}$$

where $\|\mathsf{M}^{-1}\mathsf{q}\|$ is the Euclidean norm of the (scaled) source vector $\mathsf{M}^{-1}\mathsf{q}$. With the help of this reduced-order model for the fields, the reduced-order model for the radiated power now follows as

$$P_m(\omega) = P_{\mathrm{a}}\mathrm{Re}\left\{\mathsf{e}_1^T[r(\mathsf{H}_m, \omega) + r(\mathsf{H}_m^*, \omega)]\mathsf{e}_1\right\}, \tag{15}$$

with

$$P_{\mathrm{a}} = \frac{\omega^2|p(\omega)|^2\alpha}{2} \tag{16}$$

and $\alpha = \mathsf{q}^T\mathsf{M}^{-1}\mathsf{Wq}$. We observe that *no* basis vectors v_i are required to evaluate this reduced-order model. Moreover, a *single* Krylov decomposition (13) gives SD rate approximations for *all* frequencies (or wavelengths) of interest,

that is, the method allows for frequency sweeps even in case of dispersive media. Reduced-order field approximations can also be computed using Eq. (14) and dominant quasinormal modes can be extracted from the Lanczos decomposition of Eq. (13) as well (see Sect. 3).

3 Simulations

In this section, we demonstrate the effectiveness of the proposed reduced-order modeling technique by computing the SD rate of a quantum emitter located in the vicinity of dispersive nanorods. In our first example, the emitter is positioned above a cylindrical golden nanorod, while in the second example the emitter is sandwiched between two rectangular golden nanorods which are positioned symmetrically above and below the quantum emitter. We compute the SD rate of the quantum emitter in both scenarios and determine the excited dominant quasinormal modes in each configuration as well.

3.1 Golden nanorod

As a first example, we consider a configuration similar to the one presented in [9], which consists of an electric dipole located in the vicinity of a golden nanorod (see Fig. 1). The rod has a diameter of 30 nm and a length of 100 nm and the dipole is located 10 nm above the upper surface of the rod.

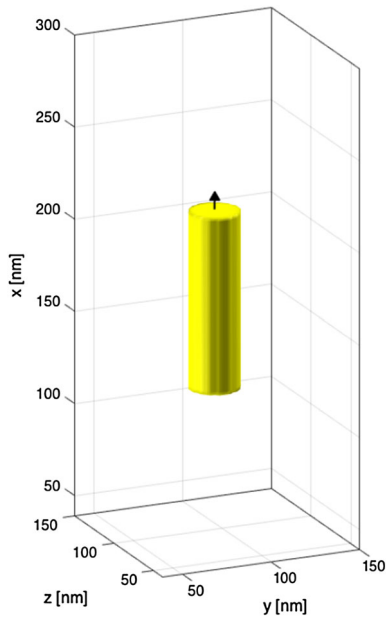

Fig. 1 A quantum emitter located above a cylindrical golden nanorod. The diameter of the rod is 30 nm and its length is 100 nm. The emitter is located 10 nm above the upper surface of the rod. The background medium has an index of refraction of $n = 1.5$ and a Drude model is used as a constitutive relation for gold

The background medium is homogeneous and is characterized by a refractive index of $n = 1.5$, while a Drude model with a plasma frequency $\omega_p = 1.26 \times 10^{16}\text{s}^{-1}$ and a collision frequency $\gamma_p = 1.41 \times 10^{14}\text{s}^{-1}$ is used as a constitutive relation for the golden nanorod. We are interested in the SD rate of the quantum emitter on a wavelength interval ranging from 0.7 to 1.2μm. Discretizing the first-order Maxwell system of Eq. (6) such that the electromagnetic field and the geometry are well resolved for all wavelengths of interest, we obtain a semidiscrete Maxwell system as given by Eq. (7) with approximately 8.7 million unknowns. Given this large order, it is clear that direct evaluation of Eq. (8) is simply not feasible. We therefore construct the reduced-order model for the radiated power as given by Eq. (15) via the Lanczos reduction algorithm. For this particular example, it turns out that a model of order $m = 4500$ is sufficient to accurately describe the SD rate of the quantum emitter over the entire wavelength interval of interest. Since the order of the original system is approximately 8.7 million, the order of the reduced-order model is about 1930 times smaller than the original system. Also note that the system matrix A is sparse, and the Lanczos algorithm is therefore very efficient, since the algorithm is based on a three-term recurrence relation and the system matrix is only needed to compute a single matrix-vector multiplication at every iteration.

Now taking the homogeneous background medium as a reference medium to compute P_0 [see Eq. (1)], we obtain the normalized decay rate curve shown in Fig. 2 (dashed curve). Also shown is the normalized SD rate as computed

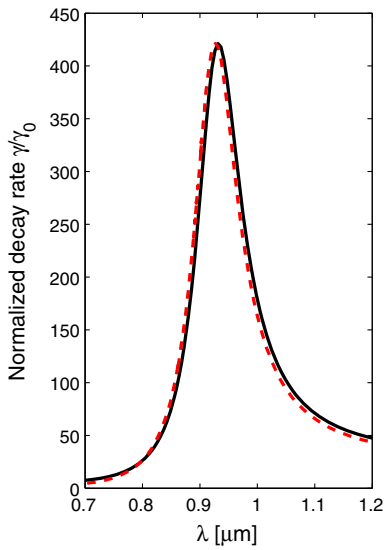

Fig. 2 Normalized spontaneous decay rate of the quantum emitter shown in Fig. 1. *Dashed line* reduced-order model of order $m = 4500$. *Solid line* normalized SD rate computed via the method proposed in [9]

in [9] (solid line). Clearly, both SD curves essentially overlap on the wavelength interval of interest.

In addition to reduced-order models for the SD rate, we can also determine the dominant quasinormal modes from the Lanczos decomposition of Eq. (13) at essentially no additional costs. Specifically, if we let (θ_j, y_j) be an eigenpair of matrix H_m then postmultiplication of the Lanczos decomposition by the eigenvector y_j leads to

$$\mathsf{A}\mathsf{z}_j = \theta_j \mathsf{z}_j + \mathsf{p}_{m+1}\mathsf{e}_m^T\mathsf{y}_j, \tag{17}$$

where $\mathsf{z}_j = \mathsf{V}_m\mathsf{y}_j$. Equation (17) shows that (θ_j, z_j) is an approximate eigenpair of the system matrix A provided $|\mathsf{e}_m^T\mathsf{y}_j|\,\|\mathsf{p}_{m+1}\|$ is small. This latter condition can be checked by direct computation (note that $\mathsf{e}_m^T\mathsf{y}_j$ is the last (mth) component of the eigenvector y_j) and quasinormal modes that dominate the SD rate response can easily be identified in this way. As an illustration, Fig. 3 shows *all* eigenvalues of the reduced Lanczos matrix H_{4500} in the complex λ-plane. The reduced-order model of Eq. (15) takes the contribution of all these eigenvalues into account, but only one eigenvalue (encircled in Fig. 3) essentially contributes to the SD rate response. The mode that corresponds to this eigenvalue has converged, and in Fig. 4 we show the magnitude of the x-component of the electric field strength of this dominant quasinormal mode for the quantum emitter configuration of Fig. 1, while Fig. 5 shows the y-component of the electric field strength. Finally, we remark that in exact arithmetic, only those modes that are excited by the emitter can be captured by the Lanczos algorithm, since the (scaled) source vector $\mathsf{M}^{-1}\mathsf{q}$ is used as a starting vector. These are the modes of interest, of course, since possible other quasinormal modes are simply not excited.

3.2 Golden nanogap antenna

As a second example, we consider a quantum emitter located at the center of a gap between two rectangular

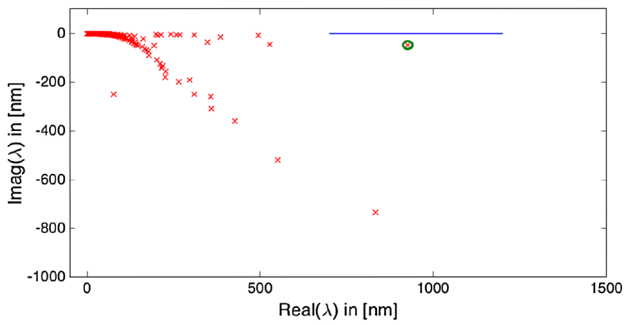

Fig. 3 Eigenvalues of the reduced-order Lanczos matrix H_{4500} (crosses) and the wavelength interval of interest (*solid line*). Only one quasinormal mode essentially contributes to the spontaneous decay rate (mode corresponding to the encircled eigenvalue)

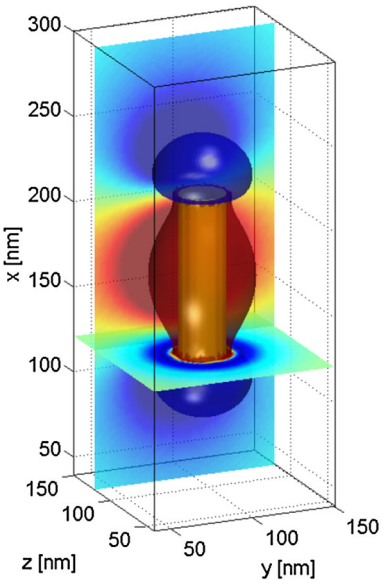

Fig. 4 Magnitude of the x-component of the electric field strength of the dominant quasinormal mode as excited by the quantum emitter of Fig. 1

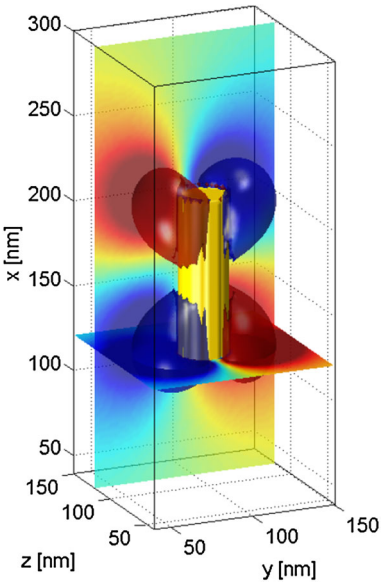

Fig. 5 Magnitude of the y-component of the electric field strength of the dominant quasinormal mode as excited by the quantum emitter of Fig. 1

golden nanorods (see Fig. 6). The side lengths of each rod are given by $28 \times 28 \times 100$ nm and the gap is 22 nm wide. We use the same Drude model as in the previous example as a constitutive relation for gold. The rods and emitter are embedded in a homogeneous background medium with a refractive index of $n = 1.5$.

Discretizing the first-order Maxwell system in space such that the electromagnetic field is well resolved for

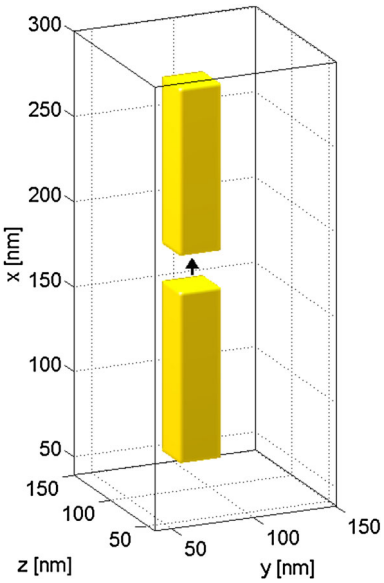

Fig. 6 A quantum emitter located at the center of a gap between two golden rectangular nanorods. The side lengths of the rods are given by $28 \times 28 \times 100$ nm, and the gap is 22 nm wide. A Drude model is used as a constitutive relation for gold, and the background medium is homogeneous with an index of refraction of $n = 1.5$

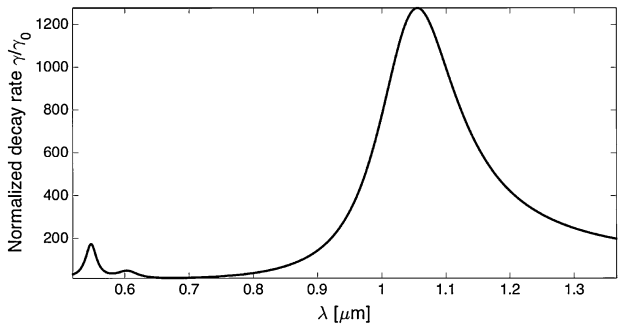

Fig. 7 Reduced-order model of order $m = 8500$ for the normalized spontaneous decay rate of the quantum emitter shown in Fig. 6

wavelengths running from 0.5 to 1.4μm, a semidiscrete Maxwell system with approximately 7.2 million unknowns is obtained. Using the Lanczos algorithm, we construct reduced-order models of increasing order until convergence is reached. For this example, a reduced-order model of order $m = 8500$ is sufficient to accurately describe the SD rate on the wavelength interval of interest (see Fig. 7). Again, the SD rate is computed by taking all eigenvalues of the reduced Lanczos matrix H_{8500} into account. However, only a small number of eigenvalues actually contribute to the SD rate in this configuration. To make this explicit, we first show all eigenvalues of H_{8500} in Fig. 8 (crosses) along with the wavelength interval of interest (solid line). The normalized SD rate based on the total reduced-order model (solid line) and the SD rate which takes only the four

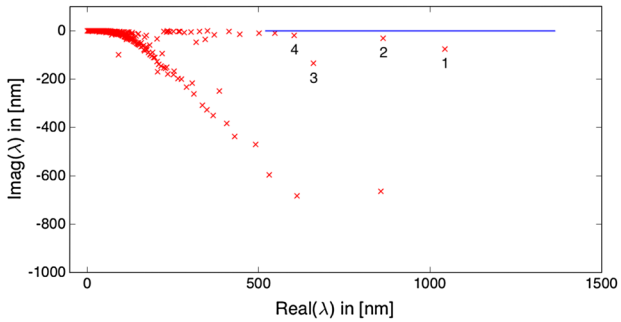

Fig. 8 Eigenvalues of the reduced-order Lanczos matrix H_{8500} (crosses) and the wavelength interval of interest (*solid line*)

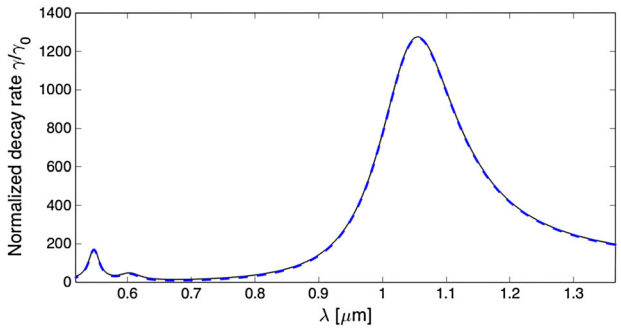

Fig. 9 SD rate of the quantum emitter in the configuration of Fig. 6. *Solid line* total reduced-order model of Fig. 7. *Dashed line* SD rate computed using only the quasinormal modes corresponding to eigenvalues 1–4 (see Fig. 8)

quasinormal modes that correspond to the eigenvalues 1 – 4 into account (dashed line) are shown in Fig. 9. We observe that a small number of quasinormal modes is already sufficient to properly capture the SD rate response of the quantum emitter over the wavelength interval of interest. Finally, in Figs. 10, 11, and 12, 13 we show the magnitude of the x- and y-components of the electric field strength of the quasinormal modes corresponding to the eigenvalues labeled 1 and 4 in Fig. 8. These modes contribute to the SD rate of the golden nanogap antenna and, as mentioned above, are determined from the Lanczos decomposition of Eq. (13).

Comparing the SD experiment for the nanorod with the experiment for the nanogap antenna, we observe that the two experiments differ not only in model complexity, but also in the wavelength range of interest. Specifically, in the nanorod experiment, only a single resonance essentially contributes to the SD rate on the wavelength interval of interest, while for the antenna, three resonance modes contribute on a wavelength interval that is larger than in the first example (smaller wavelengths are considered in the second example compared with the first). Convergence therefore slows down, since the wavelength interval and the number of modes that need to be captured is larger.

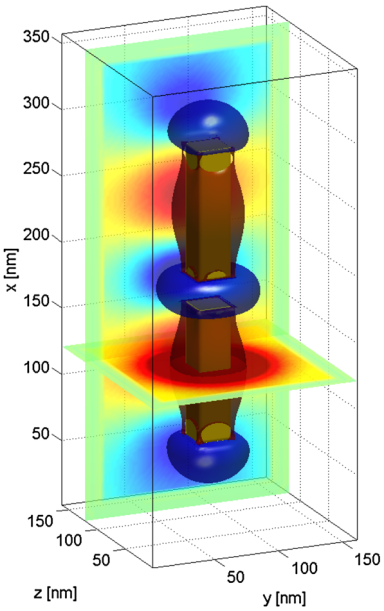

Fig. 10 Magnitude of the x-component of the electric field strength of the quasinormal mode corresponding to eigenvalue 1 of Fig. 8

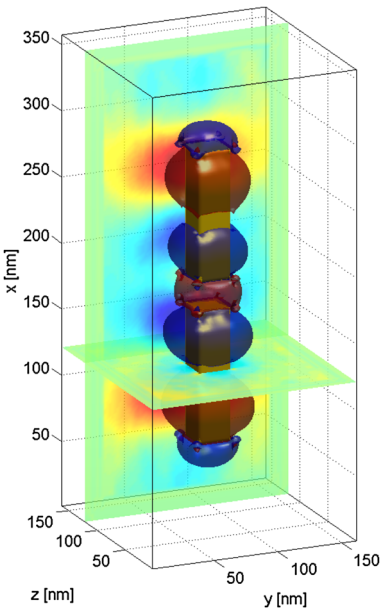

Fig. 12 Magnitude of the x-component of the electric field strength of the quasinormal mode corresponding to eigenvalue 4 of Fig. 8

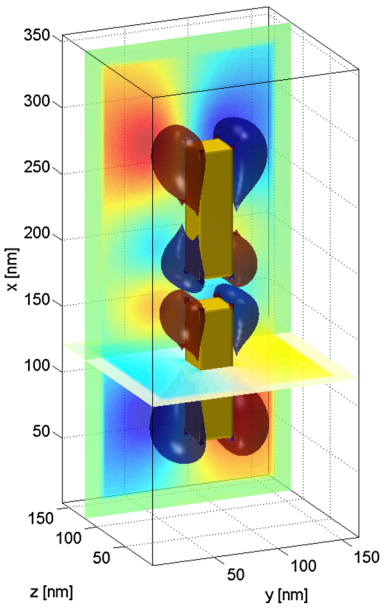

Fig. 11 Magnitude of the y-component of the electric field strength of the quasinormal mode corresponding to eigenvalue 1 of Fig. 8

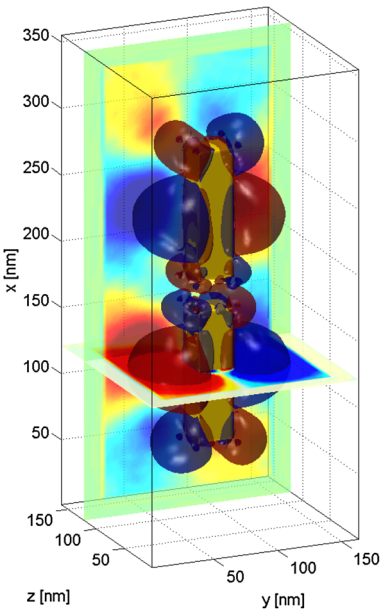

Fig. 13 Magnitude of the y-component of the electric field strength of the quasinormal mode corresponding to eigenvalue 4 of Fig. 8

Moreover, smaller wavelengths put harder constraints on the PML, which usually leads to a poorer conditioning of the system matrix.

The construction of the reduced-order model in Matlab takes about 1 h for the first example and 1.75 h for the second example on an Intel i5-3470 CPU 3.2 GHz under 64-bit Windows 7. As soon as the model is constructed, its evaluation on the complete wavelength interval of interest takes less than one second for one thousand uniformly sampled wavelength values. This "wavelength sweeping" feature is the main advantage of our reduced-order model approach.

4 Conclusions

We have presented a novel model-order reduction method to efficiently compute the spontaneous decay rate of arbitrarily shaped 3D nanosized resonators. By exploiting the symmetry of Maxwell equations in conjunction with a general second-order dispersion relation, so-called reduced-order models for the spontaneous decay rate can be constructed very efficiently via a Lanczos-type reduction algorithm. The use of this algorithm allows us to construct a single low-order model that is accurate on an entire spectral interval of interest, and frequency sweeps can be performed at negligible cost given the low order of the reduced-order models.

Large reduction factors can be achieved for general 3D resonators, since electromagnetic field responses in resonating structures are mainly dominated by a small number of quasinormal modes. Moreover, discretizing 3D resonating nanostructures in space generally leads to heavily oversampled semidiscrete Maxwell systems, since detailed subwavelength geometric features of the resonating structure need to be captured.

The small number of modes contributing to the electromagnetic response suggests the possibility of solving this problem using rational Krylov subspaces. Rational Krylov subspaces generally show superior convergence for systems with only a few contributing eigenvalues. Therefore, future work will include the design of a rational Krylov subspace algorithm to compute the electromagnetic response of 3D resonators.

We point out that the developed approach can easily be extended to multipole dispersive media in order to simulate more complex dispersive materials. For instance, a single resonator can be simulated with a dispersion relation given by the sum of a Drude and a Lorentz model. Furthermore, by storing the computed electric field strength values within the golden nanorod or by collecting the computed EM field at the boundary of the computational domain, we can determine the heat absorption or emission to the far field by invoking Poynting's theorem.

Acknowledgments The authors thank Vladimir Druskin and Mikhail Zaslavsky of Schlumberger Doll Research, MA, USA, for many stimulating discussions.

References

1. E.M. Purcell, H.C. Torrey, R.V. Pound, Resonance absorption by nuclear magnetic moments in a solid. Phys. Rev. **69**, 37–38 (1946)
2. L. Novotny, B. Hecht, *Principles of Nano-Optics* (Cambridge University Press, Cambridge, 2012)
3. A. Taflove, S. Hagness, *Computational Electrodynamics: The Finite-Difference Time-Domain Method* (Artech House, Norwood, 2012)
4. V. Druskin, R. Remis, A Krylov stability-corrected coordinate stretching method to simulate wave propagation in unbounded domains. SIAM J. Sci. Comput. **35**, B376–B400 (2013)
5. V. Druskin, S. Güttel, L. Knizhnerman, Near-optimal perfectly matched layers for indefinite Helmholtz problems. MIMS Eprints **53**, 2014 (2013)
6. V. Druskin, R. Remis, M. Zaslavsky, An extended Krylov subspace model-order reduction technique to simulate wave propagation in unbounded domains. J. Comput. Phys. **272**, 608–618 (2014)
7. J.T. Zimmerling, L. Wei, H.P. Urbach, R.F. Remis, A Lanczos model-order reduction technique to efficiently simulate electromagnetic wave propagation in dispersive media. J. Comput. Phys. (2015) **(under review)**
8. Y. Saad, *Iterative Methods for Sparse Linear Systems* (SIAM, Philadelphia, 2003)
9. C. Sauvan, J.P. Hugonin, I.S. Maksymov, P. Lalanne, Theory of the spontaneous optical emission of nanosize photonic and plasmon resonators. Phys. Rev. **110**, 237401 (2013)